Effects of Change in the Parameters of Initial Water Displacements on Energy and Amplitude Amplification of Tsunamis

Ahmad Ala Amjadi[1] and Mohammad Mokhtari[2*]

1. Ph.D. Student, International Institute of Earthquake Engineering and Seismology (IIEES), Tehran, Iran
2. Associate Professor, International Institute of Earthquake Engineering and Seismology (IIEES), Tehran, Iran, * Corresponding Author; email: mokhtari@iiees.ac.ir

ABSTRACT

In tsunami modeling, usually, the source parameter of an earthquake or landslide is computed by geophysicists, and an initial water displacement precisely similar to the seabed dislocation created by the source is obtained. Next, the initial water displacement is propagated in a predefined mesh grid using Computational Fluid Dynamics (CFD). Here, aside from the source of an earthquake or landslide, we have proposed a formula consisting of three scaling's and one rotation parameter, for creating a 3-D Initial Water Displacement (IWD). Each time one parameter was changed, and the resulting initial water displacements were modeled in a sea like modeling area. The propagated wave was recorded by the four arbitrary tide gauges at different depths near the shore. The finite difference method was used as our numerical modeling scheme in a mesh grid consisting of 100 × 150 km with an equal grid resolution of 500 m having reflective boundaries. The ratio of maximum amplitude and energy of the signal was computed in all of the arbitrary tide gauges. The results show that if an IWD is extended in the direction of the shoreline, the impact would be much lower than when the IWD is extended perpendicularly to the shoreline. The result of this study is beneficial in obtaining maximum amplitude and energy of IWD's with variable scaling and rotation parameters. Moreover, our method can be further extended to obtain charts with more values assigned to these parameters.

1. Introduction

Tsunamis are caused by various sources such as celestial impacts, huge landslides, or megathrust earthquakes in the ocean. Modeling tsunamis consists of two linked parts. First, defining the parameters of the source and calculation of the initial displacement of water (see [1] for more information). Second, modeling the propagation of the initial water displacement in a prior defined region. The main requirement for having a considerably large tsunami is the existence of the source offshore in deep water (thousands of meters). When the potential energy of a tsunami-genetic source is converted to kinetic energy, initial water displacement is generated, which has an initial velocity and a sea surface deformation similar to the co-seismic deformation [2]. The velocity is high about hundreds of kilometers per hour, and the height is usually small (few centimeters). As the wave travels to the shore, due to dispersion, its velocity is decreased within a range of smaller velocities. By approaching the shore, the dispersed waves with lower velocity meet, and their amplitude are superimposed together.

This phenomenon is called the shoaling effect and occurs when the depth of the sea becomes lesser than the wavelength (see [3] for more information). The basis of tsunami modeling is to obtain governing equations and propagate the shallow water equations within the medium. It is referred to as shallow not because we are dealing with waves in shallow water, but since the depth of the ocean is small in comparison to the wavelength of the tsunami waves generated in the deep ocean. The shallow water equations describe the governing equations of the basic hydrodynamic model for tsunami generation by disturbances on the surface [4-5]. This evolution equation derived from the theory of water waves, which approximate the behavior of real ocean, including coupled differential equations [6-8]. First, the region is discretized into grid points, and by having the value of all grid points at the initial time and implementing discretization techniques such as Finite Difference Method (FDM), we try to model the propagation of a disturbance on other nodes. We are dealing with a partial differential equation, and we want to find the value of all variables at all times. The basis of these equations and implementations are shown in the Methodology section by using a second-order Runge-Kutta method [9], which includes obtaining numerical approximations to the solution of initial value problem using the central difference scheme. Besides the materials discussed above, one must note that solving a partial differential equation (PDE) for a tsunami in any region requires a calculation time (cost). The cost varies due to the accuracy of the round-off error, grid size, and the number of grid points. Therefore, for modeling any new scenario, a new time (cost) is required. Partial differential equations of wave motion are discretized using an explicit Finite Difference Method for our analysis. One could further extend and use other numerical finite difference discretization methods such as Crank Nicolson [10], Lax Wendorff [11] and Leapfrog scheme for modeling tsunamis [12].

In this manuscript, we seek to find out the effect of changes in the initial water displacement of tsunamis. In this approach, we have proposed a formula for the initial water displacement to make the computation more compatible. The effect of changing the parameters of the proposed formula was studied by performing several numerical modeling of the IWD's in a predefined mesh grid medium.

2. Methodology

The governing equations of the shallow water wave [13] are shown in Equation (1).

$$\frac{\partial u}{\partial t} + u\frac{\partial u}{\partial x} + v\frac{\partial u}{\partial y} + g\frac{\partial \eta}{\partial x} = 0$$

$$\frac{\partial v}{\partial t} + u\frac{\partial v}{\partial x} + v\frac{\partial v}{\partial y} + g\frac{\partial \eta}{\partial y} = 0$$

$$\frac{\partial \eta}{\partial t} + \frac{\partial \left[u(h+\eta) \right]}{\partial x} + \frac{\partial \left[v(h+\eta) \right]}{\partial y} = 0 \qquad (1)$$

where x and y are horizontal coordinates, t is time, h is the still water depth, η is the vertical displacement of the water surface above still water level, u and v are water particle velocities in the x and y- directions and g is the gravitational acceleration. Two analytical and numerical methods are available to solve Equation (1). Analytical solutions provide closed-form expressions variation of dependent variables in the domain, but are only computable for specific simple geometries and are hard to compute for sophisticated domains. Numerical solutions compute values at discrete points in the domain. We use the FDM to model the shallow water equations. The underlying philosophy is to replace derivatives of governing equations with algebraic difference quotients, which results in a system of algebraic equations solvable for dependent variables at discrete grid points [14]. Consider point P in Figure 1) with coordinates(i,j), step size Δx, and Δy in x and y-direction, respectively. We can calculate the value at another point by using the Taylor series expansion [15] shown in Equation (2).

$$u_{(i+1,j)} =$$

$$u_{(i,j)} + \left(\frac{\partial u}{\partial x}\right)_{(i,j)} \Delta x + \left(\frac{\partial^2 u}{\partial x^2}\right)_{(i,j)} \frac{(\Delta x)^2}{2!} + ... +$$

$$\left(\frac{\partial^n u}{\partial x^n}\right)_{(i,j)} \frac{(\Delta x)^n}{n!} + \left(\frac{\partial^{n+1} u}{\partial x^{n+1}}\right)_{(i,j)} \frac{(\Delta x)^{n+1}}{(n+1)!} \qquad (2)$$

For a small amount of Δx higher order terms can be neglected, and by forward and backward differencing the equation, we reach to a central difference equation. The result is shown for a truncation error of $O(\Delta x)^2$ in Equation (3) where the
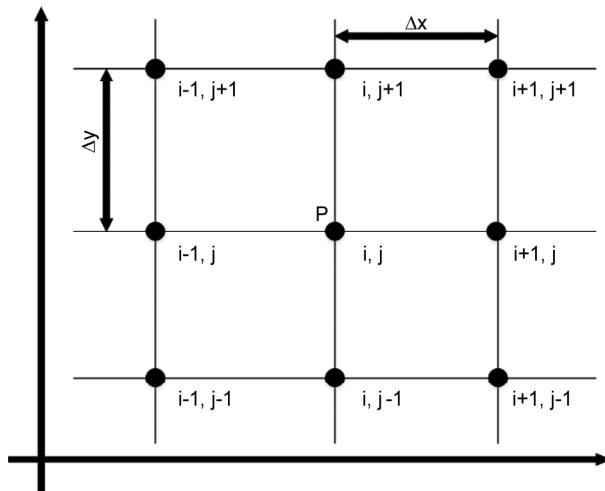
Figure 1. Representation of the Finite Difference Method Grid implemented in this study.

first derivatives of the velocity component is discretized using the central difference equation.

$$\frac{\partial u}{\partial x_{(i,j)}} = \frac{u_{(i+1,j)} - u_{(i-1,j)}}{2\Delta x} + O(\Delta x)^2 \qquad (3)$$

By substituting Equation (2) and Equation (3) in Equation (1), we can obtain values of the velocity and height at each grid points in a time marching procedure.

$$\frac{\partial u}{\partial t} = \frac{u_{(i,j)}^{n+1} - u_{(i,j)}^{n}}{\Delta t} \qquad (4)$$

For example, the value of $u_{(i,j)}^{n+1}$, which is the x-velocity of the grid point (i, j) at the time level $n+1$, can be calculated by values of u at the time level n. This time marching procedure is called the explicit method. There are other methods that the value of $u_{(i,j)}^{n+1}$ is dependent on values at time level $n+1$, which are called implicit methods that are not the basis of this study. In this manuscript, partial differential equations of wave motion are discretized using the explicit Finite Difference Method for our analysis.

2.1. Discretization of shallow water equations with explicit Finite Difference Method

For a numerical solution of the shallow water equation, the computation should be done in two separate but continuous parts. For each time level, first, the values inside the mesh grid, excluding boundaries are computed. Next, the values for the boundaries are calculated using the values of the

inner nodes. The explicit algebraic formulas are written in Equation (5).

2.1.1. Discretization for Values Inside the Mesh Grid (Excluding Boundaries)

$$u_{(i,j)}^{n+1} = \frac{u_{(i+1,j)}^{n} + u_{(i-1,j)}^{n} + u_{(i,j-1)}^{n} + u_{(i,j+1)}^{n}}{4} - \frac{1}{2}\left(\frac{\Delta t}{\Delta x}\right)\left[\frac{u_{(i+1,j)}^{n}{}^2 - u_{(i-1,j)}^{n}{}^2}{2}\right] - \frac{1}{2}\left(\frac{\Delta t}{\Delta y}\right) \times$$

$$\left[\frac{v_{(i+1,j)}^{n} u_{(i+1,j)}^{n} + v_{(i-1,j)}^{n} u_{(i+1,j)}^{n} - v_{(i+1,j)}^{n} u_{(i-1,j)}^{n} -}{2}\right.$$

$$\left.\frac{v_{(i-1,j)}^{n} u_{(i-1,j)}^{n}}{2}\right] - \frac{1}{2}g\left(\frac{\Delta t}{\Delta x}\right)\left[\frac{\eta_{(i+1,j)}^{n} - \eta_{(i-1,j)}^{n}}{2\Delta x}\right]$$

$$v_{(i,j)}^{n+1} = \frac{v_{(i+1,j)}^{n} + v_{(i-1,j)}^{n} + v_{(i,j-1)}^{n} + v_{(i,j+1)}^{n}}{4} - \frac{1}{2}\left(\frac{\Delta t}{\Delta y}\right)u_{(i,j)}^{n}\left[v_{(i+1,j)}^{n} - v_{(i-1,j)}^{n}\right] - \frac{1}{2}\left(\frac{\Delta t}{\Delta y}\right)\left[\frac{v_{(i+1,j)}^{n}{}^2 - v_{(i-1,j)}^{n}{}^2}{2}\right] - \frac{1}{2}g\left(\frac{\Delta t}{\Delta y}\right)\left[\eta_{(i+1,j)}^{n} - \eta_{(i-1,j)}^{n}\right] \qquad (5)$$

$$\eta_{(i,j)}^{n+1} = \frac{\eta_{(i+1,j)}^{n} + \eta_{(i-1,j)}^{n} + \eta_{(i,j-1)}^{n} + \eta_{(i,j+1)}^{n}}{4} - \frac{1}{2}\left(\frac{\Delta t}{\Delta x}\right)u_{(i,j)}^{n}\left[(h+\eta)_{(i+1,j)}^{n} - (h+\eta)_{(i-1,j)}^{n}\right] - \frac{1}{2}\left(\frac{\Delta t}{\Delta x}\right)(h+\eta)_{(i,j)}^{n}\left[u_{(i+1,j)}^{n} - u_{(i-1,j)}^{n}\right] - \frac{1}{2}\left(\frac{\Delta t}{\Delta y}\right)v_{(i,j)}^{n}\left[(h+\eta)_{(i+1,j)}^{n} - (h+\eta)_{(i-1,j)}^{n}\right] - \frac{1}{2}\left(\frac{\Delta t}{\Delta y}\right)(h+\eta)_{(i,j)}^{n}\left[v_{(i+1,j)}^{n} - v_{(i-1,j)}^{n}\right]$$

where U and V are the velocities in x, and y-direction, h is the still water depth, i, and j are grid points index in x and y-direction, η is the vertical distance above the still sea level in the ocean and n is the time step. The wave speed of the traveling surf is computed using Equation (6) [3], where $W_{(i,j)}$ is the wave speed at location $(i.j)$, u_0 is the initial velocity of the surf, and the last term is the velocity of the surf due to the presence of gravity. Equation (6) shows that the velocity is proportional to the root of the water column.

$$w = u_0 + \sqrt{g(h + \eta)} \qquad (6)$$

The $W_{(i,j)}$ can be related to dt using Equation (7), where c is the CFL number [16]. In explicit (time marching) schemes, any number below one can be used as the CFL number. Smaller values of CFL require finer mesh grid, while larger values require coarser grids. In this study, we have used a constant value of 0.68 for the CFL number. The $W_{(i,j)}$ term enforces dt to vary for each grid point. Therefore, all of the dt terms in Equation (5), should be replaced by $dt_{(i,j)}$ from Equation (7).

$$dt_{(i,j)} = \frac{Cdx}{W_{(i,j)}} \qquad (7)$$

At first, no motion is assumed at the time step $n = 1$ for all of the grid points. Therefore, $U^1_{(i,j)} = 0$, $V^1_{(i,j)} = 0$.

2.1.2. Discretization for Values on the Boundary of the Mesh Grid

After all the values have been computed in the previous level (except for boundaries), we compute the values at the boundaries in time step $n = 1$. Equation (8) to Equation (10) show the computation of the velocity and water column (height). Note that in each equation, the coefficients of the right-hand side are equal to the coefficient of the left-hand side, representing a complete reflective boundary. If the coefficient of the left-hand side excels the value one, the numerical modeling would be unstable, since the height and the velocity would increase rapidly. Values lesser than one, suggest a dampening boundary.

Equation (8) shows the velocity component in the x-direction (U):

$$U^{(n+1)}_{(1,j)} = \frac{5}{2}(U^{(n+1)}_{(2,j)}) - 2(U^{(n+1)}_{(3,j)}) + \frac{1}{2}(U^{(n+1)}_{(4,j)})$$

$$U^{(n+1)}_{(ni,j)} = \frac{5}{2}(U^{(n+1)}_{(ni-1,j)}) - 2(U^{(n+1)}_{(ni-2,j)}) + \frac{1}{2}(U^{(n+1)}_{(ni-3,j)})$$

$$U^{(n+1)}_{(i,1)} = \frac{5}{2}(U^{(n+1)}_{(i,2)}) - 2(U^{(n+1)}_{(i,3)}) + \frac{1}{2}(U^{(n+1)}_{(i,4)}) \qquad (8)$$

$$U^{(n+1)}_{(i,nj)} = \frac{5}{2}(U^{(n+1)}_{(i,nj-1)}) - 2(U^{(n+1)}_{(i,nj-2)}) + \frac{1}{2}(U^{(n+1)}_{(i,nj-3)})$$

Equation (9) shows the velocity component in the y-direction (V) :

$$V^{(n+1)}_{(1,j)} = \frac{5}{2}(V^{(n+1)}_{(2,j)}) - 2(V^{(n+1)}_{(3,j)}) + \frac{1}{2}(V^{(n+1)}_{(4,j)})$$

$$V^{(n+1)}_{(ni,j)} = \frac{5}{2}(V^{(n+1)}_{(ni-1,j)}) - 2(V^{(n+1)}_{(ni-2,j)}) + \frac{1}{2}(V^{(n+1)}_{(ni-3,j)})$$

$$V^{(n+1)}_{(i,1)} = \frac{5}{2}(V^{(n+1)}_{(i,2)}) - 2(V^{(n+1)}_{(i,3)}) + \frac{1}{2}(V^{(n+1)}_{(i,4)}) \qquad (9)$$

$$V^{(n+1)}_{(i.nj)} = \frac{5}{2}(V^{(n+1)}_{(i,nj-1)}) - 2(V^{(n+1)}_{(i,nj-2)}) + \frac{1}{2}(V^{(n+1)}_{(i,nj-3)})$$

Equation (10) shows the height level in the z-direction (h):

$$(h+\eta)^{(n+1)}_{(1,j)} = (\frac{5}{2})((h+\eta)^{(n+1)}_{(2,j)}) -$$
$$2((h+\eta)^{(n+1)}_{(3,j)}) + (\frac{1}{2})((h+\eta)^{(n+1)}_{(4,j)})$$

$$(h+\eta)^{(n+1)}_{(ni,j)} = (\frac{5}{2})((h+\eta)^{(n+1)}_{(ni-1,j)}) -$$
$$2((h+\eta)^{(n+1)}_{(ni-2,j)}) + (\frac{1}{2})((h+\eta)^{(n+1)}_{(ni-3,j)}) \qquad (10)$$

$$(h+\eta)^{(n+1)}_{(i,1)} = (\frac{5}{2})((h+\eta)^{(n+1)}_{(i,2)}) -$$
$$2((h+\eta)^{(n+1)}_{(i,3)}) + (\frac{1}{2})((h+\eta)^{(n+1)}_{(i,4)})$$

$$(h+\eta)^{(n+1)}_{(i,nj)} = (\frac{5}{2})((h+\eta)^{(n+1)}_{(i,nj-1)}) -$$
$$2((h+\eta)^{(n+1)}_{(i,nj-2)}) + (\frac{1}{2})((h+\eta)^{(n+1)}_{(i,nj-3)})$$

2.2. Bathymetry and the Modeling Area

Setting the bathymetry and the grid file are requirements before any tsunami modeling. As seen in the previous formulas, the height of the propagating wave is dependent on the depth of water. In general, high-resolution bathymetry files create more realistic results comparing to lower resolution bathymetry files.

For the bathymetry of the modeling area, we have used a sloped ridge, which is in contrast quite similar to the actual sea (see Figure 2). All of the boundaries are set as reflective boundaries. Meaning that the wave will bounce back after hitting a boundary, and the energy is not decayed. Figure (2) shows 120 blue and 30 brown cells. Each cell consists of 20×20 grid points. The grid resolution is 500 m in both x and y-direction. Therefore, the total plan area for CFD modeling is 150×100 km². Four
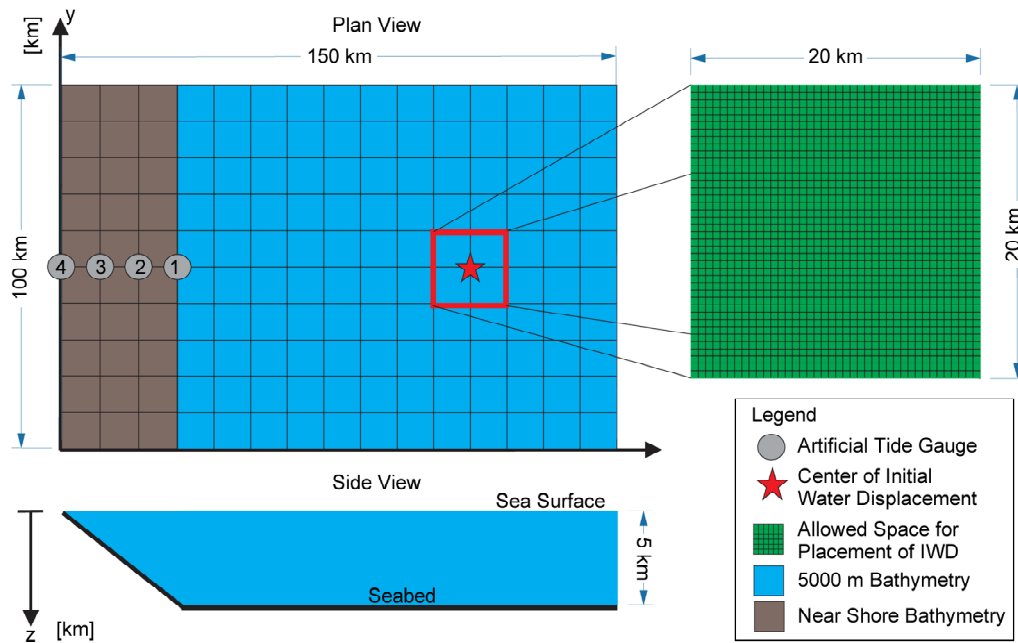
Figure 2. The plan and the side view of the mesh grid implemented in this study. The red star is the center of the Initial Water Displacement (IWD) located at a distance of 110 km and 50 km in x and y-direction from the origin. The red box contains 40×40 grid points, indicating the location for the placement from the IWD mesh grid. The grid resolution is 500 m in all the modeling area. The depth of the blue cells is 5000 m. The width of the modeling area is 100 km, and the length of the modeling area is 150 km long. The brown cells indicate depths lesser than 5000 m. The slope of the seashore is shown in the side view. The arbitrary tide gauge stations are shown by circles nominated by the number stating for the station number. Station 1 is closest to the IWD, and station 4 is the last station that receives the tsunami waves. The shoreline is the vertical line in the left of in the "Plan view", which passes through Station 4. The stations are intentionally kept in one line to illustrate the effect of bathymetry better.

arbitrary tide gauge stations are kept on the sea surface near the shore at distances 0, 10, 20, and 30 km from the y-axis. The depth of the seabed is increased linearly from 0 to 5000 m in the brown cells from the shore and is kept constant 5000 afterward (blue cells). The tide gauges are intentionally kept near the shore, to monitor the effect of initial water displacement at the various columns of waters. Station 4 is at the surface of the seabed. Station 3, 2, and 1 are at 1667 m, 3333 m, and 5000 m to the seabed, respectively.

2.3. Generating Initial Water Displacement

We propose Equation (11) to represent a typical symmetric initial water displacement. An asymmetric initial water displacement requires more additional parameters and is not the subject of this study. The parameters a, b, and c in Equation (11) are scaling parameters in z, x, and y-direction respectively.

$$z_0 = axe^{-\left(\frac{x^2}{b}+\frac{y^2}{c}\right)} \tag{11}$$

The value of z_0 in Equation (11) can produce a scaled initial water displacement. Subplots *b*, *c*, *d*, and *e* in Figure (3) shows the effect of modifications in scaling parameters. By changing the scaling parameters, the height and skewness of the initial water displacement would vary. The increase in the values of parameters a, b, and c results in an increase in z, x, and y-direction, respectively. Once the scaled initial water displacement is generated, one could use Equation (12) to apply rotation and create a rotated initial water displacement. By changing the rotation parameter 'θ' in Equation (12), the initial water displacement is rotated counterclockwise around the z-axis. In Equation (11), the X and Y are values in the new grid after rotation, x_0, and y_0 are the values of x, and y before rotation, and R is the "Rotation Vector". Subplot (*f*) in Figure (3) shows the rotation of 70 degrees counterclockwise, applied to the subplot (*e*) of Figure (3).

$$\begin{bmatrix} X \\ Y \end{bmatrix} = R \begin{bmatrix} x_0 \\ y_0 \end{bmatrix} = $$
$$\begin{bmatrix} \cos\theta_i & -\sin\theta_i \\ \sin\theta_i & \cos\theta_i \end{bmatrix} \begin{bmatrix} x_0 \\ y_0 \end{bmatrix} = $$
$$\begin{bmatrix} x_0 \cos\theta_i & -y_0 \sin\theta_i \\ x_0 \sin\theta_i & y_0 \cos\theta_i \end{bmatrix} \tag{12}$$
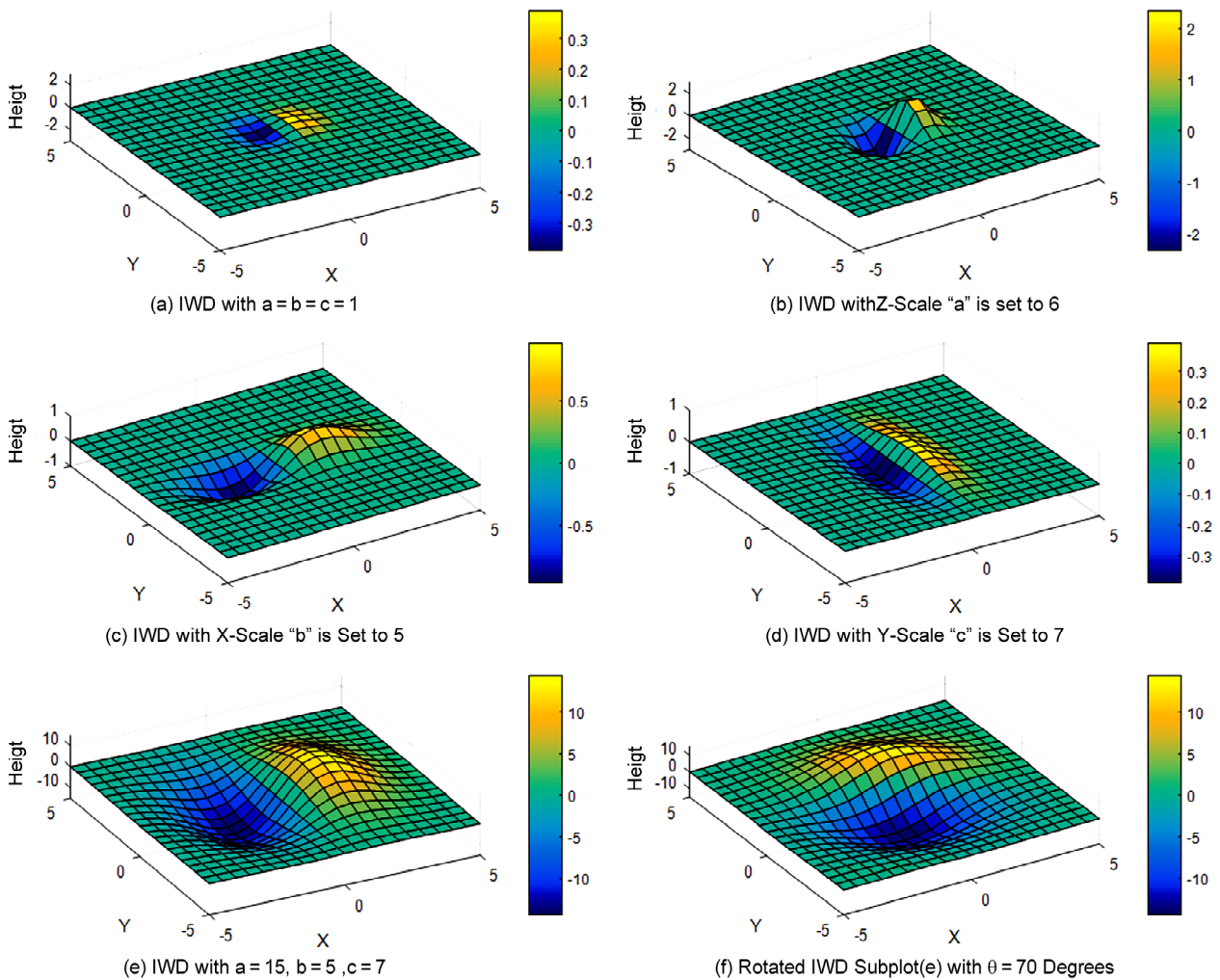
Figure 3. The plot of a 3D Initial Water Displacement (IWD) using Equation (11) and results due to the change in scaling parameters and rotation parameters using Equation (12). (a): IWD with all scaling parameters is set to 1. (b) IWD with Z-Scale or 'a' is set to 6. (c): IWD with X-Scale or 'b' is set to 5. (d): IWD with Y-Scale or 'c' is set to 7. (e): IWD with scaling parameters a=15, b=5, c=7. (f): Rotated IWD of subplot (e) 70 degrees counterclockwise.

2.4. Transferring the IWD to the Final Modeling Area and Performing CFD

The initial water displacement, which has been generated with scaling and rotation parameters, is transferred and applied to the predefined modeling area mesh grid. Subplots in Figure (3) shows a quarter of the total mesh grid area assigned for the IWD. The allowable mesh grid area for the presence of IWD is the green mesh grid in Figure (2), which consists of 40×40 grids with a resolution of 500 m. Both the IWD grid and the final modeling grid have similar grid resolutions. All of the initial velocities in x and y-direction are assumed zero. The values of the scaled and rotated initial water displacement are added to the predefined modeling mesh at the appropriately assigned nodes. By performing these actions, the initial condition is applied to the modeling area, and the CFD model is ready for execution. In the CFD modeling, the height and the velocity components are computed at all of the grid points at all of the time steps. A predefined time is considered to terminate the CFD process.

3. Results and Discussion

Let name the IWD of Figure (3a) as the "Mother IWD". A CFD was modeled using the Mother IWD as the surface of water elevation before propagation, and the arbitrary tide gauges have recorded the tsunami signal. Let name the generated records by the "Mother IWD" as "Mother Records 1" to 4 (Figure 4). The maximum amplitudes of "Mother records" were measured 5.0170, 5.1983, 5.1784 and 3.5464 cm for Mother records 1 ,2, 3, and 4, respectively. The considerable smaller value recorded at station 4 is due to the presence of the arbitrary tide gauge station at a reflective boundary.
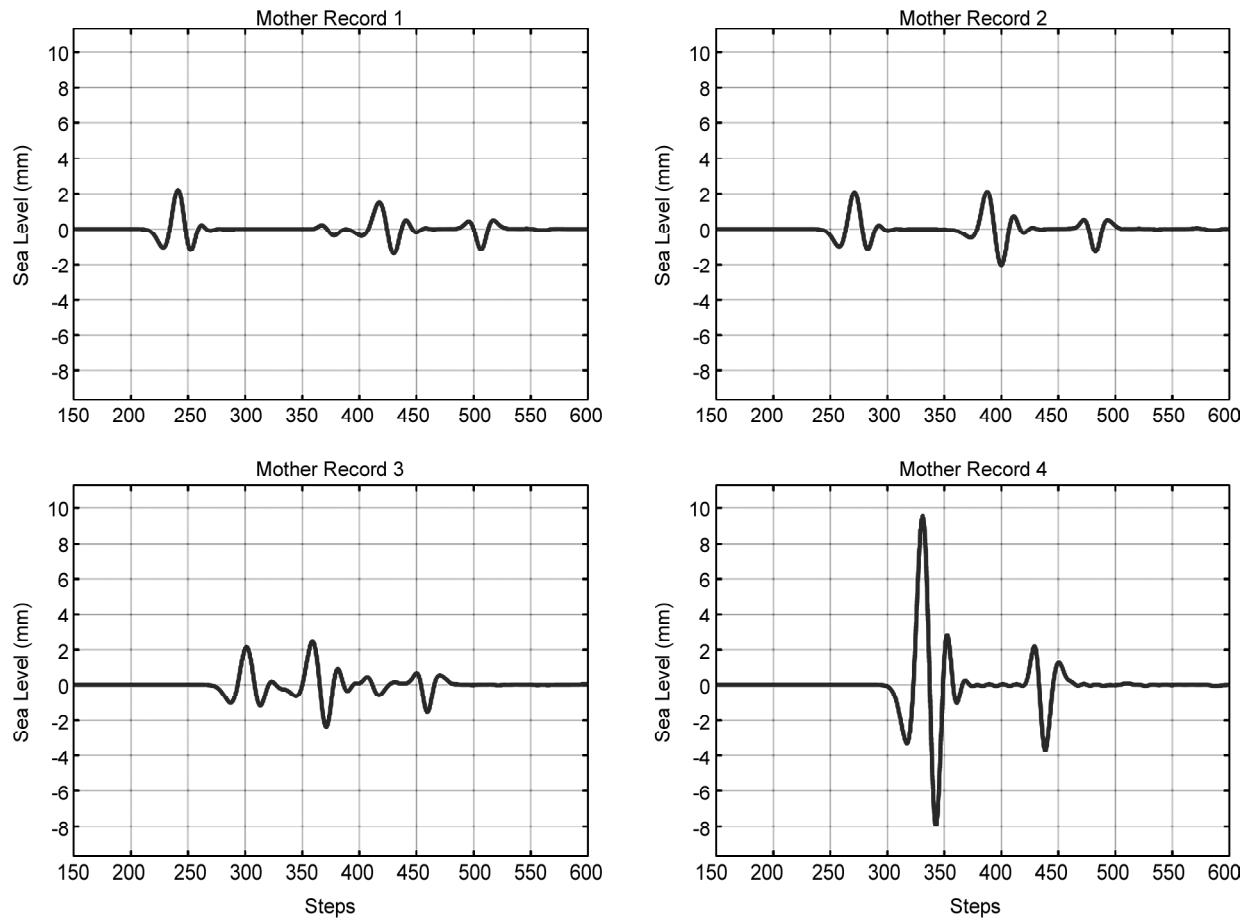
Figure 4. Mother Records as a result of applying the Mother IWD in the modeling area. Mother Records 1-3 barely reach the amplitude of 5 mm, but Mother Record 4 exceeds an amplitude of 17 mm. The secondary wave in Mother Record 4 (Steps 420-480) is an example of a reflected wave from a reflective boundary. These reflected waves have smaller amplitude in comparison with the initial impact. The reflected waves are also present in the Mother records 1-3. There is a slight amplitude amplification for stations 1 to 3 and this is much more amplified in station 4.

At reflective boundaries, the signal is reflected, and a portion of the signal is attenuated. This results in smaller amplitude, and the energy of the signal is reduced due to this effect. Figure (4) shows that, by approaching the shore, the duration of the signal is decreased (the signal is tightened), and the amplitude is increased (slightly). The increase of the amplitude of a tsunami wave by approaching the shore is due to the shoaling effect. This phenomenon occurs when the amplitude of the traveling wave is smaller than the depth of the water column.

The cumulative energy of the Mother Records was computed using Equation (13), where x_n is the discrete values of the height difference from the sea level recorded by the arbitrary tide gauges. Note that the term "energy" is for characterizing the tide gauge signals and is not the actual measurement of the energy of the signal. The unit of the cumulative energy is (unit of signal)^2.

$$E_s = \langle x_n . x_n \rangle = \sum_{-\infty}^{+\infty} |x_n|^2 \tag{13}$$

Values 0.90275 E-4, 0.11940 E-3, 0.15362 E-3, and 0.12 E-2 were obtained for the four arbitrary tide gauge stations one to four, respectively. Figure (5) shows the cumulative energy of the tide gauges. By approaching the shore, the amplitude of the tsunami wave is increased, causing an amplification in the energy of the tsunami wave. When the tsunami waves hit a reflective boundary, the amplitude of the wave decreases, and the energy of the wave is decayed. The cumulative energy plots in Figure (5) show the incremental process of the cumulative energy of the tsunami wave for the four arbitrary tide gauges. When a tsunami wave hits the arbitrary tide gauge until when it passes completely, there is a considerable increment in the cumulative energy plot. After the tsunami wave passes the arbitrary tide gauge
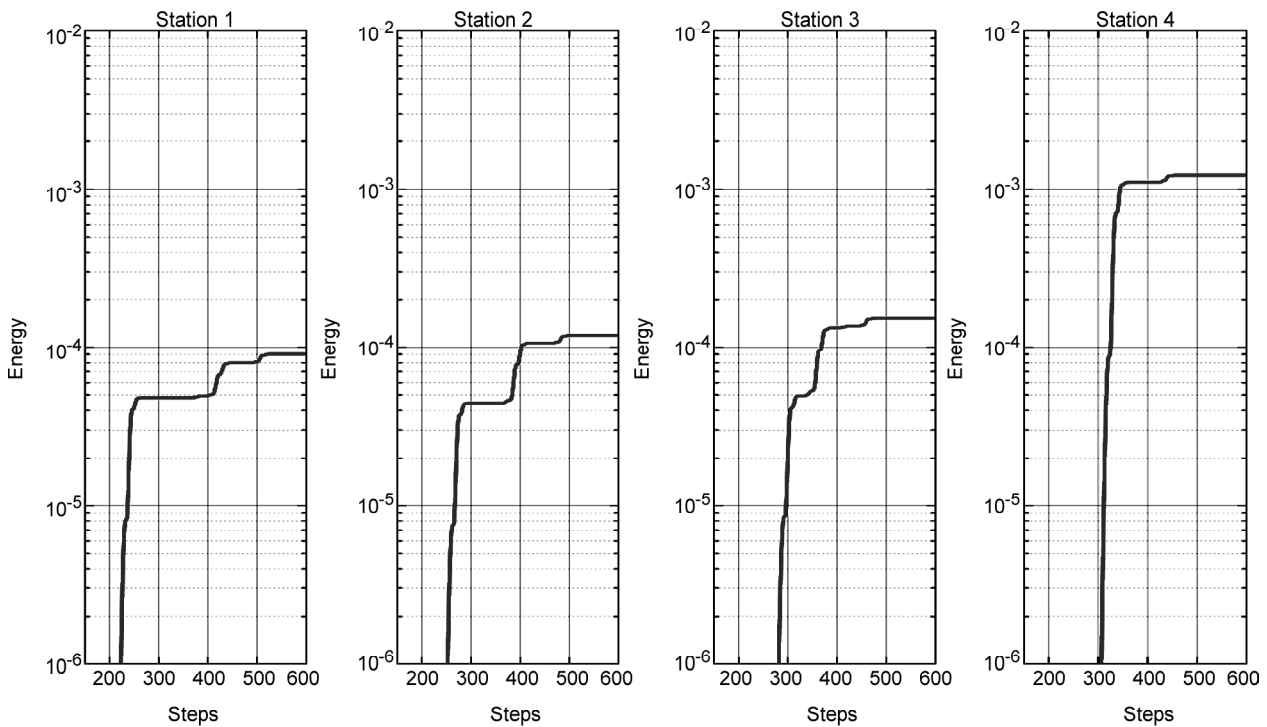
Figure 5. Presentation of the cumulative energy of the Mother records recorded at arbitrary tide gauge stations; the vertical scale is logarithmic. The values lesser than 10E-6 are not shown. The places where the energy is a straight horizontal line, there is no movement at that station. Small increments can easily detect the hit of secondary reflected waves after the first large increment.

station, it hits a reflective boundary and reflects until it reaches again to the arbitrary tide gauge station. Before the second hit with the tide gauge station, there is no increment in the cumulative energy plots. The hit with a reflective boundary decreases the amplitude severely. Therefore, the energy plots do not rise to excessively higher values after the first hit of the tsunami waves.

By having the value and the energy of the 'Mother Records', we can compare the effect of scaling and rotation parameters with these results. The three upper rows of Figure (6) show the effect of changes in the scaling parameters '*a*', '*b*', and '*c*', while the last row shows the effect of changes in rotation parameter 'θ'. Each change in the scaling parameters requires a separate CFD modeling in the region. Therefore, several CFD was attained for the achievement of Figure (6). Increasing the scaling parameter, '*a*' increases the ratio of amplitude with the same coefficient of '*a*'. However, the ratio of energy is increased with a higher slope and exceeds fifty for '*a* = 7' and above. All of the stations are amplified in amplitude and energy similarly. Increasing the scaling parameter '*b*' increases the ratio of amplitude with slightly higher than the value of coefficient '*b*'. However, the

ratio of energy increases to a much higher slope and exceeds one hundred for '*b*' = 7 and above. For values 1 to 5 of parameter '*b*', all of the stations are amplified in amplitude and energy similarly. Nevertheless, increasing the value of '*b*' Station 4, which is closer to the shore, receives lesser amplification in amplitude and energy than other stations. Increasing the scaling parameter '*c*' increases the ratio of amplitude slighter than any other scaling parameter. The maximum value achieved is 3 in amplitude, and is quite nonlinear for the amplitude amplification ratio, but seems linear for the ratio of energy. The maximum ratio of energy amplification is approximately 10 for '*c* = 10'. Therefore, the '*c*' parameter receives minimal value in comparison to other scaling parameters. Increasing the rotation parameter 'θ' from zero to 90 degrees decreases the ratio of amplitude and energy. After 90 to 180 degrees, the ratio of amplitude and energy is increased again periodically. The periodic change is visible, and two periods are shown in the last row of Figure (6). Figure (6) can be used as a chart to estimate the combined values of scaling and rotation parameters. For example, if we assign any values between 1 to 10 for scaling parameters and 0 to 360 for the
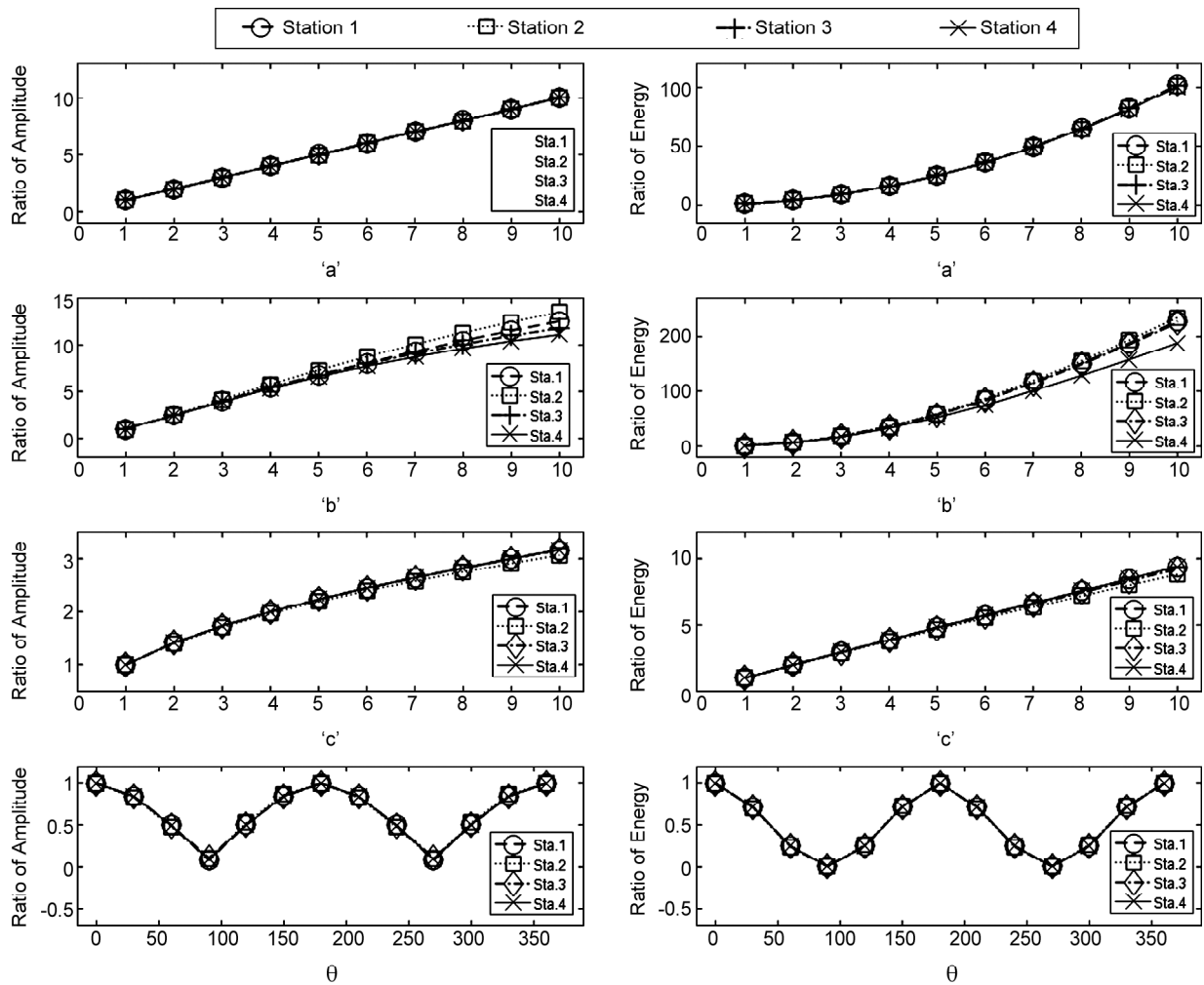
Figure 6. Effects of the change in scaling and rotation parameters of an initial water displacement caused by a tsunami; The left and the right column shows the effects of the change on amplitude and energy, respectively. The top three rows are results of changes in parameters 'a', 'b', and 'c', while the last row is the results of changes in the rotation parameter 'θ'. The symbols in the legend are the place where the values are calculated. For each station, a curve is fitted through the values.

rotation parameter, then one could obtain the maximum amplitude and energy of the present IWD by multiplying the value obtained from the Mother IWD for amplitude (Figure 4) and energy (Figure 5), with the ratios obtained from Figure (6). In further studies, the work done here can be extended to calculate results for values more than 10.

4. Conclusion

In this manuscript, we have studied the effect of changing scaling and rotation parameters by using Initial Water Displacements (IWD's), similar to IWD's generated by tsunamis. We have proposed an equation for generating the initial water displacement. By testing several values for the scaling and rotation parameters from 1 to 10, we have clearly shown that the scaling parameters '*a*' (height or z-scale) and '*b*' (x-scale) better amplify

the amplitude and energy of the incoming wave in comparison to the scaling parameter '*c*' (y-scale) which has the lowest impact on amplification of amplitude and energy. Meaning that if an IWD is extended in the shoreline direction, the impact is much lower when the same IWD is extended perpendicularly to the shoreline direction. The results of this study can be used in the estimation of the maximum amplitude and energy of initial water displacements, by multiplying the ratio of amplitude and energy coefficients to the prior values of mother IWD's.

Acknowledgments

References

1. Okada, Y. (1985) Surface deformation due to shear and tensile faults in a half-space. *Bulletin of the Seismological Society of America*, **75**(4), 1135-1154.

2. Bolshakova, A., Nosov, M., and Kolesov, S. (2015) The properties of co-seismic deformations of the ocean bottom as indicated by the slip-distribution data in tsunamigenic earthquake sources. *Moscow University Physics Bulletin*, **70**(1), 62-67.

3. Ward, S.N. (2011) *Tsunami Encyclopedia of Solid Earth Geophysics*. Springer, 1473-1493.

4. Akylas, T. (1984) On the excitation of long nonlinear water waves by a moving pressure distribution. *Journal of Fluid Mechanics*, **141**, 455-466.

5. Nosov, M. and Skachko, S. (2001) Nonlinear tsunami generation mechanism. *Natural Hazards and Earth System Science*, **1**(4), 251-253.

6. Grilli, S., Guyenne, P., and Dias, F. (2000) Numerical Computation of three-dimensional ovreturning waves. *15st International Workshop on Water Waves and Floating Bodies*, **59**.

7. Layton, A.T., and van de Panne, M. (2002) A numerically efficient and stable algorithm for animating water waves. *The Visual Computer*, **18**(1), 41-53.

8. Pelinovsky, E., Talipova, T., Kurkin, A., and Kharif, C. (2001) Nonlinear mechanism of tsunami wave generation by atmospheric disturbances. *Natural Hazards And Earth System Science*, **1**(4), 243-250.

9. Butcher, J. (2007) Runge-Kutta methods. *Scholarpedia*, **2**(9), 3147.

10. Crank, J. and Nicolson, P. (1947) A practical method for numerical evaluation of solutions of partial differential equations of the heat-conduction type. *Paper presented at the Mathematical Proceedings of the Cambridge Philosophical Society.*

11. Lax, P. and Wendroff, B. (1960) Systems of conservation laws. *Communications on pure and applied mathematics*, **13**(2), 217-237.

12. Goto, C., Ogawa, Y., Shuto, N., and Imamura, F. (1997) IUGG/IOC time project: Numerical method of tsunami simulation with the leap-frog scheme. *Intergovernmental Oceanographic Commission of UNESCO, Manuals and Guides*, 35.

13. Dawson, T.H. (1976) *Governing Equations of Motion Theory and Practice of Solid Mechanics*, Springer., 47-70.

14. Bergman, T.L. and Incropera, F.P. (2011) F*undamentals of Heat and Mass Transfer*. John Wiley & Sons.

15. Taylor, B. (1715) *Methodus Incrementorum Directa & Inversa*. Auctore Brook Taylor: Typis Pearsonianis: Prostant Apud Gul. Innys.

16. Courant, R., Friedrichs, K., and Lewy, H. (1967) On the partial difference equations of mathematical physics. *IBM Journal of Research and Development*, **11**(2), 215-234.